Icarus 359 (2021) 114322

Contents lists available at ScienceDirect

Icarus

journal homepage: www.elsevier.com/locate/icarus

Experimental investigation of structural OH/H_2O in different lunar minerals and glass via solar-wind proton implantation

Hong Tang [a,b,c], Xiongyao Li [a,b,c,*], Xiaojia Zeng [a], Yang Li [a,b,c], Wen Yu [a,b,c], Bing Mo [a,b,c], Jianzhong Liu [a,b,c], Shijie Wang [d], Yongliao Zou [e]

[a] Center for Lunar and Planetary Sciences, Institute of Geochemistry, Chinese Academy of Sciences, Guiyang 550081, China
[b] CAS Center for Excellence in Comparative Planetology, China
[c] Key Laboratory of Space Manufacturing Technology, Chinese Academy of Sciences, Beijing 100094, China
[d] State Key Laboratory of Environmental Geochemistry, Institute of Geochemistry, Chinese Academy of Sciences, Guiyang 550081, China
[e] National Space Science Center, Chinese Academy of Sciences, Beijing 100190, China

ARTICLE INFO

Keywords:
Lunar water
Infrared spectra
Solar wind
H^+ implantation

ABSTRACT

The possibility of OH/H_2O formation on the lunar surface has been proposed because of the interaction between protons from the solar wind and oxygen in the regolith. In this study, we examined olivine, pyroxene, plagioclase, and volcanic glass samples together irradiated with 7 keV H^+ at a dose of 10^{17} ions/cm^2 under the same experimental conditions to simulate the solar-wind proton implantation process on the Moon. By comparing the infrared spectral characteristics of these samples before and after H^+ implantation through an infrared spectrometer, we confirm that OH forms in all minerals and glass after H^+ implantation, with a remarkable amount of OH/H_2O found in plagioclase. This indicates that plagioclase can capture more H^+ than other silicate phases to form the OH/H_2O. The absorption characteristics of OH/H_2O formed by H^+ implantation are distinct and associated with the mineral structure. The efficiency of OH/H_2O formation by H^+ implantation is affected by crystal structure. We conclude that OH/H_2O formed by solar-wind implantation in the lunar soil is likely to be mainly preserved in plagioclase, and the estimated OH/H_2O absorption strength from 0.7 to 3.6% at 3356 cm^{-1} and from 0.9 to 4.8% at 3622 cm^{-1} of plagioclase is consistent with those found by recent lunar spacecraft missions.

1. Introduction

The Moon has been considered bone dry ever since the Apollo era. However, this long-held view was recently challenged by mounting evidence of water (the presence of H-bearing species, such as OH and H_2O, hereafter referred to simply as "water") from remote sensing and lunar sample analyses (Boyce et al., 2010; McCubbin et al., 2010; Greenwood et al., 2011; Hauri et al., 2011; Hui et al., 2013; Barnes et al., 2014; Hayne et al., 2015; Robinson et al., 2016). Remarkable absorption characteristics at about 3 μm and 2.8 μm on almost the entire lunar surface were detected by onboard infrared (IR) spectrometers on the Cassini, Deep Impact, and Chandrayaan-1 missions (Clark, 2009; Sunshine et al., 2009; Pieters et al., 2009; Li and Milliken, 2017; Wöhler et al., 2017; Bandfield et al., 2018), which indicated the presence of H_2O and OH, respectively. The widespread OH/H_2O on the lunar surface has been thought to be the result of solar-wind proton implantation (e.g., Pieters et al., 2009). Specifically, when solar-wind protons are implanted into the minerals, protons are captured in the crystal structure and can bond with the oxygen of silicate minerals in the lunar regolith. Experiments of ion irradiation over a range of energies (0.5 keV to a few MeV) have indicated that ion irradiation could lead to the breaking of chemical bonds within various minerals (e.g., Futagami et al., 1990; Demyk et al., 2001; Davoisne et al., 2008). The implanted or trapped protons from the solar wind could attach to those broken bonds and form OH and subsequently H_2O (Burke et al., 2011; McCord et al., 2011). The process has been investigated by a series of laboratory experiments determining whether the proton irradiation of minerals could form OH/H_2O. Most of these results demonstrated the possibility of the solar-wind proton origin of lunar OH/H_2O (Djouadi et al., 2011; Managadze et al., 2011; Ichimura et al., 2012; Bradley et al., 2014; Schaible and Baragiola, 2014). However, the samples, the fluence and energy of implanted ions in these experiments were different, which could not compare the

* Corresponding author at: Center for Lunar and Planetary Sciences, Institute of Geochemistry, Chinese Academy of Sciences, Guiyang 550081, China.
E-mail address: lixiongyao@vip.skleg.cn (X. Li).

https://doi.org/10.1016/j.icarus.2021.114322
Received 8 July 2020; Received in revised form 3 January 2021; Accepted 4 January 2021
Available online 15 January 2021

abundance and occurrence of solar wind-induced water in different minerals and glass. Liu et al. (2012) analysed the Apollo 11 and 17 lunar samples using Fourier-transform infrared spectroscopy (FTIR) and secondary ion mass spectroscopy. This work revealed the presence of hydroxyl that is equivalent to 70–200 ppm H_2O in lunar agglutinitic glasses. The hydrogen isotope compositions of some agglutinitic glasses (i.e., $\delta D < -700‰$) suggested that the hydroxyl is associated with the solar wind source (i.e., $\delta D \approx -1000‰$). However, the occurrence and abundance of water formed by solar-wind implantation on the Moon and their differences in major lunar minerals are still ambiguous. This study aims to address these questions. According to the components of the lunar regolith, four different samples (i.e., olivine, pyroxene, plagioclase, and volcanic glass) were used as lunar analogue samples for H^+ implantation under the same conditions. The absorption characteristics of structural OH/H_2O formed in these samples and the effects of the mineral structure on the OH/H_2O formation were analysed. Also, the possible occurrence of structural OH/H_2O formation implanted by solar-wind protons on the Moon was discussed.

2. Samples and experiments

Lunar regolith is mainly composed of silicate minerals and glass. The most common silicate minerals are plagioclase, pyroxene, and olivine (Heiken et al., 1991). These mineral phases have been exposed to the solar wind for a long period, and OH/H_2O can form in the surface of these minerals by capturing protons. To investigate the formation mechanism of OH/H_2O by solar-wind implantation on the Moon, terrestrial olivine, pyroxene, plagioclase, and glass were therefore chosen as the lunar analogue samples. This study focused on revealing the difference in water formation by solar-wind implantation in various lunar minerals and glass. Thus, we believe it is reasonable to use terrestrial minerals and glass for experimental investigation.

The olivine and pyroxene were separated respectively from peridotite and pyroxenite xenoliths from the Damaping volcanic field in Hebei, China. Olivine grains were mainly composed of forsterite (Fo = 89–100) and the pyroxene samples consisted of orthopyroxene (En = 74–75) and clinopyroxene (Wo = 49–50). The studied plagioclase (An = 50–53) was taken from Damiao anorthosite in Hebei, China. Dacitic glass sample used in this work was sourced from volcanic glass in Changbaishan, Jilin, China.

Quantitative chemical compositions of the studied minerals and glass were determined using a JEOL JXA-8230 electron microprobe (EMP) analyser at the Guilin University of Technology. It was operated at an accelerating voltage of 15 kV and electron beam current of 20 nA. Both natural and synthetic standards were used and matrix corrections were based on ZAF procedures. The data are listed in Table 1. For quantitative analysis of the water content in these samples, doubly polished thin sections were prepared before the experiments. The thickness of samples section about 150–350 μm. To reduce the effect of adsorbed water on the sample surface, the thin sections were baked at 110 °C for 24 h before ion implantation.

To simulate the process of solar-wind implantation on the Moon, an ion implanter was used to implant H^+ into the samples. The experiments were performed at the Center for Lunar and Planetary Sciences (CLPS), Institute of Geochemistry, Chinese Academy of Sciences. The ion implanter comprises an ion source, vacuum system, magnetic analyser, accelerator, sample chamber, and control system (see Fig. 1). In this study, all the samples were placed together in a sample holder of the vacuum chamber to guarantee they were subjected to the same doses of radiation. The chamber was evacuated, purged with high-purity nitrogen (99.999%), and then maintained at a pressure of 2.25×10^{-6} Torr at 22 °C before implantation. The H_2 gas had a purity of 99.999%. The magnetic analyser ensured that a flow of only H^+ was allowed to enter the sample area. The samples were irradiated with H^+ at 7 keV, which is higher than the average energy (~1 keV) of solar wind. This is limited by instrumental conditions; however, this energy can be used in this study

Table 1
Major and minor compositions of the studied minerals and glass.

	Olivine	Orthopyroxene	Clinopyroxene	Plagioclase	Glass
SiO_2	41.00 ± 0.19	52.50 ± 0.19	49.70 ± 0.22	56.60 ± 0.54	66.90 ± 0.30
Al_2O_3	0.02 ± 0.02	4.90 ± 0.09	6.44 ± 0.17	25.70 ± 0.36	15.00 ± 0.20
MgO	46.70 ± 0.23	25.60 ± 0.32	12.40 ± 0.17	b.d.	0.17 ± 0.02
TFeO	9.92 ± 0.15	15.20 ± 0.15	6.60 ± 0.14	0.16 ± 0.04	5.15 ± 0.14
CaO	0.08 ± 0.02	0.53 ± 0.02	22.00 ± 0.13	10.10 ± 0.96	1.51 ± 0.33
Na_2O	b.d.	0.02 ± 0.01	0.78 ± 0.06	5.08 ± 0.32	3.27 ± 0.46
TiO_2	b.d.	0.15 ± 0.01	0.87 ± 0.04	0.09 ± 0.02	0.46 ± 0.06
K_2O	0.02 ± 0.01	b.d.	b.d.	0.86 ± 0.22	6.41 ± 0.07
MnO	0.11 ± 0.02	0.20 ± 0.06	0.07 ± 0.02	b.d.	0.13 ± 0.01
NiO	0.44 ± 0.02	b.d.	b.d.	b.d.	b.d.
Cr_2O_3	0.04 ± 0.01	0.09 ± 0.03	0.17 ± 0.02	b.d.	b.d.
P_2O_5	b.d.	b.d.	b.d.	b.d.	b.d.
Total	98.32	99.22	99.06	98.67	99.05

Major and minor element data expressed as oxide wt%. Errors for major and minor elements are 1σ standard deviations. Each sample was measured for 3–5 times.
b.d. = below detection limit.

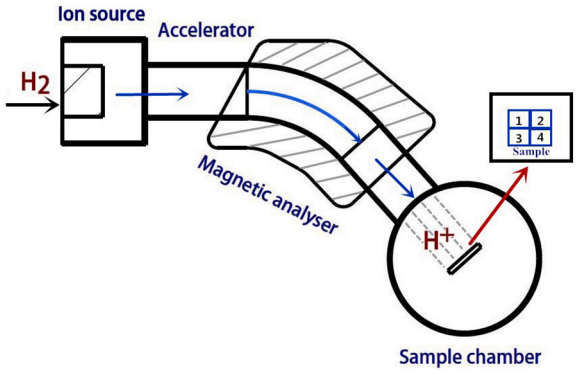

Fig. 1. The schematic of ion implanter.

to compare the differences of water production between various minerals and glass. The implanted H^+ dose was 10^{17} ions/cm^2, which corresponded to an exposure time of about 17 years on the Moon (Burke et al., 2011). The flux was approximately 2.3×10^{12} ions/cm^2·s. During the process of implantation, the pressure of the chamber was maintained at 5.5×10^{-5} Torr.

To examine the OH/H_2O formation in these samples, micro-FTIR AIM 8000 at Institute of Geochemistry, Chinese Academy of Sciences was used to measure IR transmission spectra under a high-purity nitrogen protected environment. The implanted samples were exposure in air less than 10 min during the transfer from the irradiation chamber to the IR spectrometer. Clean, crack-free, and alteration-free areas on each pure mineral crystal were chosen for IR measurements. Each measurement spot size was a diameter of 50 μm in size. To evaluate the exact change in the IR absorption characteristics, the same positions were analysed before and after ion implantation. The IR spectra were obtained in the range of 2000–7000 cm^{-1} (1.43–5 μm) on each sample using 256 scans, with a spectral resolution of 2 cm^{-1}.

3. Results and discussion

After H^+ implantation, the colour of all the samples is darkened in irradiated region. The IR spectra (2500–4500 cm^{-1}) of the studied minerals and glass are presented in Fig. 2. Our results show that the main change before and after ion implantation is located in the range of 3300–3700 cm^{-1}, which is caused by the fundamental O—H stretch absorption of water and hydroxyl. To determine the influence of environmental water on the implanted samples, an olivine sample was irradiated by 7 keV He^+ with 10^{17} ions/cm^2 as the background sample. Fig. 2f showed that the absorption about 3400 cm^{-1} disappeared, which was caused by the sputtering of H in the surface of the olivine sample during the He^+ irradiation. Thus, the increased absorption of water in each implanted sample is attributed entirely to the implanted H^+ rather than the adsorption of atmospheric water. Comparing the IR spectra after irradiation to those before irradiation, plagioclase shows the most pronounced change, and the variations in the other minerals and glass are relatively small. The position, strength and shape of the absorption peak are also different among these minerals and glass. This indicates that OH/H_2O is formed in the olivine, orthopyroxene, clinopyroxene, plagioclase, and glass by H^+ implantation, although the ability and occurrence of OH/H_2O formation in these minerals and glass are

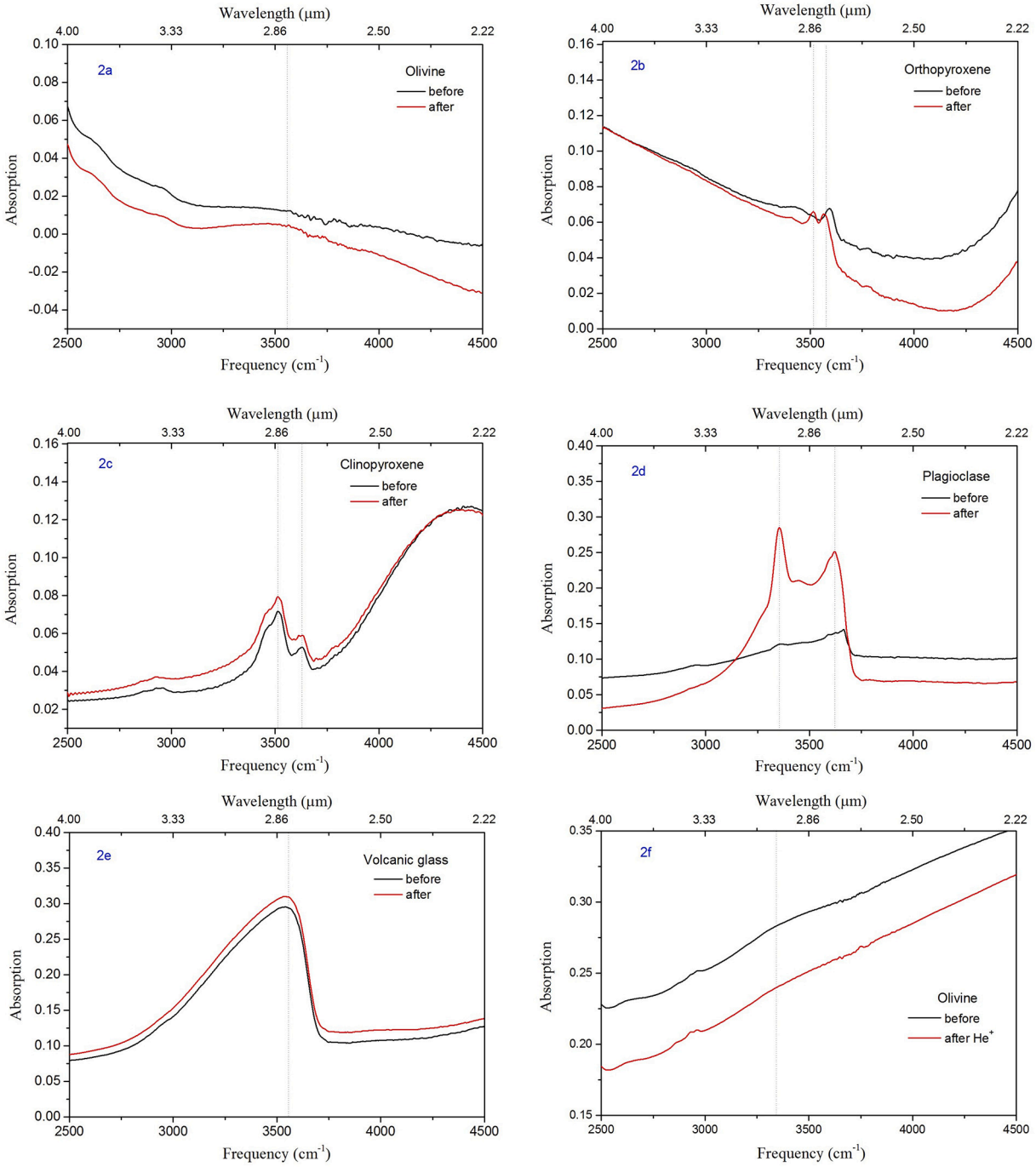

Fig. 2. IR spectra of the studied samples before (black) and after (red) irradiation. The olivine, orthopyroxene, clinopyroxene, plagioclase, and glass reveal different variations in the range of 3300–3700 cm^{-1}, especially the remarkable variations seen in plagioclase. The absorption at ~2900 cm^{-1} for C—H bands in some samples are organic contamination during the preparation of doubly polished thin sections. (For interpretation of the references to colour in this figure legend, the reader is referred to the web version of this article.)

different.

3.1. Difference of OH/H_2O formation in IR spectra

Compared to the IR spectra before H^+ irradiation, new peak positions at 3564 and 3518 cm^{-1} are observed in the IR spectra of olivine and orthopyroxene after H^+ irradiation, respectively (see Table 2). For olivine, the new peak shows a broad wave number range with the centre at 3564 cm^{-1}. The peak position and shape in irradiated olivine are similar to those in Schaible and Baragiola (2014). Lemaire et al. (2004) demonstrated that the absorption in the range of 3450–3620 cm^{-1} in forsterite is attributed to OH groups associated with Si sites. Thus, the presence of a new broad peak indicates that a new OH is formed in the silica tetrahedron. After H^+ implantation, a portion of implanted H ions combines with oxygen in the tetrahedron and then forms OH. In addition, the broad peak indicates that OH forms in the amorphous structure, which is caused by H^+ irradiation. For orthopyroxene, with the new peak at 3518 cm^{-1}, it is also interpreted that OH forms in the tetrahedra, identical to the findings of Rauch and Keppler (2002). Except for the two new peak positions, other peaks in orthopyroxene (at ~3560 cm^{-1}), clinopyroxene, plagioclase and glass after H^+ implantation are relatively higher, identical to the original peak positions. This implies that the formation of these peak positions is preferential and they retain OH/H_2O via H^+ irradiation.

In addition, the peak positions in orthopyroxene, clinopyroxene, plagioclase, and glass generally move toward smaller wave numbers after H^+ implantation. That is, the absorption peak is redshifted. This implies that the absorption strength of the O—H bond is weakened, which is closely related to the crystal deformation. As shown in Table 2, it can be seen that the shift in the two absorption peaks is different in clinopyroxene and plagioclase. The smaller wave number absorption peak corresponding to OH in the tetrahedron has a relatively small shift compared to the larger wave number absorption peak corresponding to OH in the other site where protons are attached to the O_2Mg oxygen atom (Rauch and Keppler, 2002).

Corresponding to the change in peak position, the peak strengths of all these minerals and glass enhance after H^+ implantation. Plagioclase shows the most remarkable change in IR spectra compared to the other minerals and glass. This implies that OH formation is easier in plagioclase than the other minerals and glass when they are implanted with H^+ at the same energy and dose of radiation. For plagioclase, the absorption peaks at 3622 and 3356 cm^{-1} correspond to the H_2O (structurally bound water molecule) and OH mentioned by Johnson and Rossman (2004), respectively.

3.2. Effect of mineral structure on OH/H_2O abundance

Based on Beer–Lambert law, the water content in the studied samples can be calculated as follows:

$$A = 1/3 \times \varepsilon' \times c \times d \text{ (for anisotropic mineral)} \quad (1)$$

$$H = c \times d \times \rho \times \varepsilon/(18 \times 1000) \text{ (for glass)} \quad (2)$$

where A and H are the integrated absorbance expressed as the integrated absorption area (in cm^{-1}) and absorption height, respectively, ε' is the integral absorption coefficient (in $ppm^{-1}\cdot cm^{-2}$), ε is the molar absorption coefficient ($L\cdot mol^{-1}\cdot cm^{-1}$), c is the water content (in ppmw), d is the thickness of the sample (in cm), ρ is the density (2.50 g/cm^3 for glass here), and 1/3 is the orientation factor for non-polarized measurement (Paterson, 1982). The uncertainty of the calculated water content was estimated to be ~20%–30% for the uncertainties in sample thickness, spectra baseline correction, unpolarized light measurements, and the absorption coefficient (Kovács et al., 2008; Liu et al., 2012). Spectrum processes including baseline correction and absorption calculations are performed by OMNIC software.

The changes in water content in these samples are presented in Table 3. Although there are some intrinsic differences in water content among these minerals and glass, there is a clear increasing trend after H^+ implantation.

For olivine, there is barely any water before H^+ implantation for no absorption in the IR spectra, whereas the water content reaches 16 ± 1 ppm after H^+ implantation. The water is considered to form in the silica tetrahedron for H^+ compensating the charge defects in Si vacancies. Lemaire et al. (2004) suggested that the absorption peaks at 3613 ± 2, 3580 ± 2, and 3566 ± 2 cm^{-1} are attributed to the vibration of OH in different orientations. When H^+ is located along the O—O edge of the tetrahedron, absorption is seen at 3580 ± 2 and 3566 ± 2 cm^{-1}.

For pyroxene, a small change in water content is shown after H^+ implantation in both orthpyroxene and clinopyroxene. A new absorption peak at 3518 cm^{-1} is found in orthopyroxene after H^+ implantation, corresponding to the formation of water (i.e., 9 ± 1 ppm). In contrast, the other absorption peak at 3594 cm^{-1} existing in orthopyroxene before H^+ implantation exhibits little change in water content after being implanted with H^+. Similarly, little change in absorption strength at the peak of the larger wave number (i.e., 3630 cm^{-1}) is observed in clinopyroxene after H^+ implantation. The increase in water content with 36 ± 7 ppm in clinopyroxene corresponds to the change in absorption peak at 3514 cm^{-1}. According to the previous works (Rauch and Keppler, 2002; Katayama and Nakashima, 2003; Koch-Müller et al., 2004; Skogby, 2006), absorption peaks at about 3520 and 3549 cm^{-1} are caused by OH formation for Al^{3+}+H^+ substituting Si^{4+} in the tetrahedron. In this studied samples, the Al content is about 0.8 and 1.1 at.% in orthopyroxene and clinopyroxene, respectively. Most of Al^{3+} replaces Si^{4+} and leads to a charge imbalance in the tetrahedron. When the mineral is implanted by H^+, it is favourable for the tetrahedron to form OH by capturing H^+ to compensate the charge imbalance. This view is confirmed in our experiment where the OH increases in the tetrahedron, corresponding to absorption peaks at 3518 and 3514 cm^{-1} in the orthopyroxene and clinopyroxene after H^+ implantation, respectively.

As shown in Table 3, the water content increases most remarkably in plagioclase after H^+ implantation. It is estimated to be 158 ± 19 and 187 ± 27 ppm at 3356 and 3622 cm^{-1}, respectively. As in previous work by Johnson and Rossman (2004), the absorption peak at 3622 cm^{-1} in plagioclase is correlated with the H_2O (structurally bound water molecule). In the crystal boundary and vesicles within the amorphous rims mentioned by Bradley et al. (2014), there are many oxygen-dangling bonds, and a local charge imbalance is produced. To compensate the charge balance, those oxygen-dangling bonds are favourable for capturing H^+ and forming H_2O. The peak of OH at 3356 cm^{-1} in plagioclase is aligned with the crystallographic α axis (Johnson and

Table 2
Absorption characteristics of the mineral IR spectra.

	Olivine		Orthopyroxene		Clinopyroxene		Plagioclase		Glass	
	Before	After	Before	After	Before	After	Before	After	Before	After
Peak Position (cm^{-1})	–	3564	3594	3568	3630	3616	3668	3622	3546	3538
			–	3518	3514	3512	3368	3356		
Peak Strength (%)	–	1.3	1.2	1.4	0.8	0.9	3.4	12.2	19.1	19.3
			–	0.6	2.5	2.6	0.5	9.0		

'–': No spectra peak.

Table 3
Water content calculated with IR absorption characteristics in minerals and glass.

Minerals	ΔH (%)/ ΔA (cm^{-1})	d (cm)	ε ($ppm^{-1}\cdot cm^{-2}$)	Δc (ppm)	Peak position (cm^{-1})	occurrence
Olivine	0.872	0.0315	5.09 ± 0.33[a]	16 ± 1	−/3564	OH
Orthopyroxene	0.695	0.0150	15.60 ± 0.94[b]	9 ± 1	−/3518	OH
	0.079			1 ± 1	3568/3594	OH
Clinopyroxene	1.286	0.0150	7.09 ± 0.32[b]	36 ± 7	3512/3514	OH
	0.039			1 ± 1	3616/3630	OH
Plagioclase	26.987	0.0175	29.3 ± 3[c]	158 ± 19	3356/3368	OH
	31.972			187 ± 27	3622/3668	H_2O
Volcanic glass	0.2*	0.0225	62.32 ± 0.42**	10 ± 1	3538/3546	OH

Notes: 'ΔH' and 'ΔA' represent the changes in height and area of the absorption peak, respectively; 'd' represents thickness of the studied samples; 'ε' represent the absorption coefficient of the mineral; 'Δc' represent the water content change.
[a] Data from Bell et al. (2003);
[b] Data from Bell et al. (1995);
[c] Data from Mosenfelder et al. (2015);
* ΔH;
** The units are $L\cdot mol^{-1}\cdot cm^{-1}$ (Mandeville et al., 2002).

Rossman, 2004). The OH formation mechanism is similar to pyroxene in which Si^{4+} is substituted by Al^{3+}+H^+ in the tetrahedron.

Based on the discussion above, the OH/H_2O formed by H^+ implantation strongly depends on the local charge imbalance in the mineral structure. Compared to the crystalline minerals, glass might have fewer charge imbalance defects. Thus, it is more difficult to capture H^+ and form OH/H_2O by implantation. In our experiment, glass shows a water content change of only 10 ± 1 ppm after H^+ implantation. It seems contrary to the Apollo agglutinitic glass, which contains about 200 ppm of hydroxyl formed by solar-wind implantation (Liu et al., 2012). The reason for this is that the formation mechanism of water (OH) in agglutinitic glass is different from that in mineral phases. Considering that the origin of lunar agglutintic glass is multiple impact melting, the OH was not only formed directly by solar-wind implantation, but also by complex processes (i.e., by proton implantation followed by micrometeorite melting and mixing). However, in terms of lunar silicate minerals, the formation of OH in these phases is mainly related to the defects produced after H^+ implantation (i.e., solar-wind implantation). Plagioclase belongs to the framework silicate and has the largest surface density of the silica tetrahedron among the three silicate minerals. Therefore, it can capture much more H^+ in the tetrahedron than olivine and pyroxene. Based on the change in water content, the capture ratio of H^+ to form OH/H_2O is estimated to be 0.009%, 0.006%, 0.021%, 0.19%, and 0.006% for olivine, orthopyroxene, clinopyroxene, plagioclase, and glass after being implanted with 10^{17} ions/cm^2 of H^+, respectively.

3.3. OH/H_2O formation by solar-wind implantation on the moon

On the lunar surface, H_2O and OH species can be formed when solar-wind protons interact with the oxygen-rich lunar soil particles. Plagioclase is an important component in the lunar soil and ranges from 12.9 to 69.1 vol% (Heiken et al., 1991), and it is favourable to form OH/H_2O by solar-wind proton implantation. Assuming all the OH/H_2O is formed in plagioclase when the soil particles are implanted by solar-wind protons on the lunar surface, the absorption strength of the IR spectra of lunar soil (H_s) can be inferred by the following function:

$$H_s = H \cdot \frac{d_s}{D} \cdot S \quad (3)$$

Here, H is the height of the absorption peak in irradiated plagioclase sample, D is the thickness of the plagioclase sample in cm, d_s is the lunar soil particle size in cm, and S is the plagioclase content in the lunar soil.

For the average particle size of 100 μm, when the plagioclase content varies from 12.9 to 69.1%, the absorption strength of the lunar soil according to formula (3) changes from 0.7 to 3.6% at 3356 cm^{-1} and from 0.9 to 4.8% at 3622 cm^{-1}. This is consistent with the previous spacecraft exploration results. First, the Moon Mineralogy Mapper (M^3) on Chandrayaan-1 detected the strongest OH/H_2O absorption signal at several fresh feldspathic craters (Pieters et al., 2009) and found that lunar mare exhibits weaker H_2O/OH absorption than the lunar highlands (Wöhler et al., 2017). Although there is ongoing debate on these observations (e.g., Li and Milliken, 2017; Bandfield et al., 2018), our results suggest that OH/H_2O formed by solar-wind implantation in the lunar soil is likely to be preferentially preserved in plagioclase-rich highland area. Second, the variation in absorption strength with plagioclase abundance is consistent in spectra from the Visual and Infrared Mapping Spectrometer (VIMS) on Cassini, the M^3 on Chandrayaan-1, and the Deep Impact High-Resolution Instrument-infrared spectrometer (HRIIR). It shows absorption strength of about 2–3% near 2.8 μm in the VIMS (Clark, 2009). With HRIIR data, Sunshine et al. (2009) found that the 2.8 μm absorption strength ranges from 9 to 11% for the lunar mare and 10 to 12% for the highlands along the lunar morning terminator, which is the strongest absorption in a lunar day. In the M^3 data, the absorption strength of about 3 μm is mostly <4% below latitude of about 45° versus 2.8 μm mainly from 3 to 6% along the full lunar latitude (Pieters et al., 2009; McCord et al., 2011).

4. Conclusions

In this study, olivine, pyroxene, plagioclase, and glass phases are implanted with 7-keV H^+ at a dose of 10^{17} ions/cm^2 under the same radiation conditions. The IR spectrum analyses of these samples show that structural OH/H_2O is formed after H^+ implantation, and the structural OH/H_2O content in plagioclase is the highest. The characteristics of absorption are different among these minerals and glass associated with different structures. In crystalline minerals, structural OH/H_2O formation after H^+ implantation is mainly related to the tetrahedron defects. Plagioclase belongs to the framework silicate and has the largest surface density of silica tetrahedra among the three silicate minerals. Therefore, it can capture much more H^+ in tetrahedra and thus form the most OH compared to other minerals. Our experimental results suggest that the structural OH/H_2O formed by solar-wind implantation in the lunar soil is preferentially preserved in plagioclase. We calculate that for an average particle size of 100 μm, the absorption strength of the lunar soil changes from 0.7 to 3.6% at 3356 cm^{-1} and from 0.9 to 4.8% at 3622 cm^{-1} when the plagioclase content varies from 12.9 to 69.1 vol %, which is consistent with the results from recent spacecraft exploration missions. This study could be helpful in understanding the differences in the formation processes and abundance of OH/H_2O in different silicate minerals and glass on airless bodies (e.g., the Moon, Mercury). Our results will also aid the interpretation of variations in OH/H_2O abundance recently observed by infrared spectra from Cassini, Deep Impact, and Chandrayaan-1. It could also improve understanding of

surficial OH/H_2O detection by infrared spectrometers in the Chang'e-3/4 lunar in-situ exploration missions and the Chang'e-5 lunar sample return mission.

Declaration of Competing Interest

None.

Acknowledgements

This work was supported by the Strategic Priority Research Program of Chinese Academy of Sciences (XDB 41000000), National Natural Science Foundation of China (number 41773066, 41931077); Youth Innovation Promotion Association CAS (2018435), Technical Advanced Research Project of Civil Space (D020201), Key Research Program of Frontier Sciences (QYZDY-SSW-DQC028), Beijing Municipal Science and Technology Commission (Z181100002918003), and Guizhou Province Science and Technology Fund ([2013]2288 and [2020]1Z035). We thank Qingzhu Yin for his helpful comments that increased the quality of the paper.

Appendix A. Supplementary data

Supplementary data to this article can be found online at https://doi.org/10.1016/j.icarus.2021.114322.

References

Bandfield, J.L., Poston, M.J., Klima, R.L., Edwards, C.S., 2018. Widespread distribution of OH/H_2O on the lunar surface inferred from spectral data. Nat. Geosci. 11, 173–177.
Barnes, J.J., Tartèse, R., Anand, M., McCubbin, F.M., Franchi, I.A., Starkey, N.A., Russell, S.S., 2014. Widespread distribution of OH/H_2O on the lunar surface inferred from spectral data. Earth Planet. Sci. Lett. 390, 244–252.
Bell, D.R., Ihinger, P.D., Rossman, G.R., 1995. Quantitative analysis of trace OH in garnet and pyroxenes. Am. Mineral. 80, 465–474.
Bell, D.R., Rossman, G.R., Maldener, J., Endisch, D., Rauch, F., 2003. Hydroxide in olivine: a quantitative determination of the absolute amount and calibration of the IR spectrum. J. Geophys. Res. 108, 2105.
Boyce, J.W., Liu, Y., Rossman, G.R., Guan, Y.B., Eiler, J.M., Stolper, E.M., Taylor, L.A., 2010. Lunar apatite with terrestrial volatile abundances. Nature 466, 466–469.
Bradley, J.P., Ishii, H.A., Gillis-Davis, J.J., Ciston, J., Nielsen, M.H., Bechtel, H.A., Martin, M.C., 2014. Detection of solar wind-produced water in irradiated rims on silicate minerals. PNAS 111, 1732–1735.
Burke, D.J., Dukes, C.A., Kim, J.-H., Shi, J., Famá, M., Baragiola, R.A., 2011. Solar wind contribution to surficial lunar water: laboratory investigations. Icarus 211, 1082–1088.
Clark, R.N., 2009. Detection of adsorbed water and hydroxyl on the moon. Science 326, 562–564.
Davoisne, C., Leroux, H., Frère, M., Gimblot, J., Gengembre, L., Djouadi, Z., Ferreiro, V., d'Hendecourt, L., Jones, A., 2008. Chemical and morphological evolution of a silicate surface under low-energy ion irradiation. A&A 482, 541–548.
Demyk, K., Carrez, P., Leroux, H., Gordier, P., Jones, A.P., Borg, J., Quirico, E., Raynal, P. I., d'Hendecourt, L., 2001. Structural and chemical alteration of crystalline olivine under low energy He^+ irradiation. A&A 368, L38–L41.
Djouadi, Z., Robert, F., d'Hendecourt, L.L.S., Mostefaoui, S., Leroux, H., Jones, A.P., Borg, J., 2011. Hydroxyl radical production and storage in analogues of amorphous interstellar silicates: a possible "wet" accretion phase for inner telluric planets. A&A 531, A96.
Futagami, T., Ozima, M., Nakamura, Y., 1990. Helium ion implantation into minerals. Earth Planet. Sci. Lett. 101, 63–67.
Greenwood, J.P., Itoh, S., Sakamoto, N., Warren, P., Taylor, L., Yurimoto, H., 2011. Hydrogen isotope ratios in lunar rocks indicate delivery of cometary water to the moon. Nature Geosic. 4, 79–82.
Hauri, E.H., Weinreich, T., Saal, A.E., Rutherford, M.C., Orman, J.A.V., 2011. High pre-eruptive water contents preserved in lunar melt inclusions. Science 333, 213–215.
Hayne, P.O., Hendrix, A., Sefton-Nash, E., Siegler, M.A., Lucey, P.G., Retherford, K.D., Williams, J.-P., Greenhagen, B.T., Paige, D.A., 2015. Evidence for exposed water ice in the Moon's south polar regions from lunar reconnaissance orbiter ultraviolet albedo and temperature measurements. Icarus 255, 58–69.
Heiken, G.H., Vaniman, D.T., French, B.M., 1991. Lunar sourcebook: a user's guide to the moon. Cambridge University Press, pp. 121–181.
Hui, H., Peslier, A.H., Zhang, Y., Neal, C.R., 2013. Water in lunar anorthosites and evidence for a wet early moon. Nat. Geosci. 6, 177–180.
Ichimura, A.S., Zent, A.P., Quinn, R.C., Sanchez, M.R., Taylor, L.A., 2012. Hydroxyl (OH) production on airless planetary bodies: evidence from H^+/D^+ ion-beam experiments. Earth Planet. Sci. Lett. 345–348, 90–94.
Johnson, E.A., Rossman, G.R., 2004. A survey of hydrous species and concentrations in igneous feldspars. Am. Mineral. 89, 586–600.
Katayama, I., Nakashima, S., 2003. Hydroxyl in clinopyroxene from the deep subducted crust: evidence for H_2O transport into the mantle. Am. Mineral. 88, 229–234.
Koch-Müller, M., Matsyuk, S.S., Wirth, R., 2004. Hydroxyl in omphacites and omphacitic clinopyroxenes of upper mantle to lower crustal origin beneath the Siberian platform. Am. Mineral. 89, 921–931.
Kovács, I., Hermann, J., O'Neill, H.S.C., Fitz Gerald, J., Sambridge, M., Bor Horvat, H.G., 2008. Quantitative absorbance spectroscopy with unpolarized light: Part II. Experimental evaluation and development of a protocol for quantitative analysis of mineral IR spectra. Am. Mineral. 93, 765–778.
Lemaire, C., Kohn, S.C., Brooker, R.A., 2004. The effect of silica activity on the incorporation mechanisms of water in synthetic forsterite: a polarized infrared spectroscopic study. Contrib. Mineral. Petrol. 147, 48–57.
Li, S., Milliken, R.E., 2017. Water on the surface of the moon as seen by the moon mineralogy mapper: distribution, abundance, and origins. Sci. Adv. 3, e1701471.
Liu, Y., Guan, Y., Zhang, Y., Rossman, G.R., Eiler, J.M., Taylor, L.A., 2012. Direct measurement of hydroxyl in the lunar regolith and the origin of lunar surface water. Nat. Geosci. 5, 779–782.
Managadze, G.G., Cherepin, V.T., Shkuratov, Y.G., Kolesnik, V.N., Chumikov, A.E., 2011. Simulating OH/H_2O formation by solar wind at the lunar surface. Icarus 215, 449–451.
Mandeville, C.W., Webster, J.D., Rutherford, M.J., Taylor, B.E., Timbal, A., Faure, K., 2002. Determination of molar absorptivities for infrared absorption bands of H_2O in andesitic glasses. Am. Mineral. 87, 813–821.
McCord, T.B., Taylor, L.A., Combe, J.-P., Kramer, G., Pieters, C.M., Sunshine, J.M., Clark, R.N., 2011. Sources and physical processes responsible for OH/H_2O in the lunar soil as revealed by the Moon Mineralogy Mapper (M^3). J. Geophys. Res. 116. E00G05.
McCubbin, F.M., Steele, A., Hauri, E.H., Nekvasil, H., Yamashita, S., Hemley, J., 2010. Nominally hydrous magmatism on the moon. Proc. Natl. Acad. Sci. U. S. A. 107, 11223–11228.
Mosenfelder, J.L., Rossman, G.R., Johnson, E.A., 2015. Hydrous species in feldspars: a reassessment based on FTIR and SIMS. Am. Mineral. 100, 1209–1221.
Paterson, M.S., 1982. The determination of hydroxyl by infrared absorption in quartz, silicate glasses and similar materials. Bull. Mineral. 105, 20–29.
Pieters, C.M., Goswami, J.N., Clark, R.N., Annadurai, M., Boardman, J., Buratti, B., Combe, J.-P., Dyar, M.D., Green, R., Head, J.W., Hibbitts, C., Hicks, M., Isaacson, P., Klima, R., Kramer, G., Kumar, S., Livo, E., Lundeen, S., Malaret, E., McCord, T., Mustard, J., Nettles, J., Petro, N., Runyon, C., Staid, M., Sunshine, J., Taylor, L.A., Tompkins, S., Varanasi, P., 2009. Character and spatial distribution of OH/H_2O on the surface of the moon seen by M^3 on Chandrayaan-1. Science 326, 568–572.
Rauch, M., Keppler, H., 2002. Water solubility in orthopyroxene. Contrib. Mineral. Petrol. 143, 525–536.
Robinson, K.L., Barnes, J.J., Nagashima, K., Thomen, A., Franchi, I.A., Huss, G.R., Anand, M., Taylor, G.J., 2016. Water in evolved lunar rocks: evidence for multiple reservoirs. Geochim. Cosmochim. Acta 188, 244–260.
Schaible, M.J., Baragiola, R.A., 2014. Hydrogen implantation in silicates: the role of solar wind in SiOH bond formation on the surfaces of airless bodies in space. J. Geophys. Res. 119, 2017–2028.
Skogby, H., 2006. Water in natural mantle minerals I: pyroxenes. Rev. Mineral. Geochem. 62, 155–167.
Sunshine, J.M., Farnham, T.L., Feaga, L.M., Groussin, O., Merlin, F., Milliken, R.E., A'Hearn, M.F., 2009. Temporal and spatial variability of lunar hydration as observed by the Deep Impact spacecraft. Science 326, 565–568.
Wöhler, C., Grumpe, A., Berezhnoy, A.A., Shevchenko, V.V., 2017. Time-of-day-dependent global distribution of lunar surficial water/hydroxyl. Sci. Adv. 3, e1701286.